



ELSEVIER

Available online at [www.sciencedirect.com](http://www.sciencedirect.com)

SCIENCE @ DIRECT®

Journal of Crystal Growth 279 (2005) 276–288

JOURNAL OF **CRYSTAL  
GROWTH**

[www.elsevier.com/locate/jcrysgro](http://www.elsevier.com/locate/jcrysgro)

# On three-dimensional instability of a traveling magnetic field driven flow in a cylindrical container

Alexander Yu. Gelfgat\*

*School of Mechanical Engineering, Faculty of Engineering, Tel-Aviv University, Ramat Aviv, Tel-Aviv 69978, Israel*

Received 18 November 2004; accepted 16 February 2005

Available online 31 March 2005

Communicated by J.J. Derby

## Abstract

Three-dimensional instability and patterns of an axisymmetric flow of electrically conducting liquid in a cylindrical enclosure driven by an axial traveling magnetic field (TMF) is studied. The attention is focused on the TMF of a large axial wavenumber or large frequency, which leads to a formation of the skin layer near the sidewall. It is shown that the flow intensity grows with the increase of the TMF wavenumber from small to a moderate value and decreases with further increase of the wavenumber. Similar dependence of the flow intensity on the growing TMF frequency is observed. The critical amplitude of the electromagnetic forcing, which corresponds to a transition from axisymmetric to three-dimensional flow state, sharply decreases with the increase of the TMF wavenumber or frequency from a small value. After reaching a minimum it slowly increases with the further increase of the wavenumber or frequency.

© 2005 Elsevier B.V. All rights reserved.

PACS: 81.05.Cy; 81.10.Fq; 81.10.Mx; 47.15.Fe; 47.20.Gv; 47.62.+q

Keywords: A1. Electromagnetic flow control; A1. Flow stability; B2. Semiconductor melts

## 1. Introduction

The traveling magnetic field (TMF) is one of the various tools which can be used for the electromagnetic control of melt flows in bulk semiconductor crystal growth. Conversely to the widely used rotating magnetic field (RMF), the TMF

yields a possibility to create or control meridional melt circulations directly, i.e., without unnecessary forcing of a non-uniform rotational flow [1,3]. This possibility initiated a number of recent studies devoted to the TMF-driven and TMF-controlled flows regarding various crystal growth applications in terrestrial and microgravity environment [1–11].

One of the important problems directly connected with the TMF driving and control of melt

\*Tel.: +97236407207; fax: +97236407443.

E-mail address: [gelfgat@eng.tau.ac.il](mailto:gelfgat@eng.tau.ac.il).

flows in crystal growth processes is the stability of the resulting time-average flow. The study of this issue was started in Ref. [11], where the simplest possible expression for the TMF driving force was used. The model considered in Ref. [11] corresponds to small dimensionless TMF wavenumbers  $\alpha$  and small dimensionless circular frequency  $\gamma$ , and does not account for a possible skin-effect. The present study extends results of Ref. [11] to the cases of moderate and large wavenumbers. The TMF-driven flow in a cylindrical container is considered. In the following, we discuss how the time-averaged TMF force and the TMF-driven flow patterns change with the growth of TMF wavenumber. Then we study the three-dimensional stability of axisymmetric TMF-driven flows for different aspect ratios of the container and the TMF wavenumber varying from 1 to 20. Another parameter, which can affect the TMF driving force, is so-called skin depth  $K = \sqrt{\gamma}$  [4], where  $\gamma$  can be interpreted also as a dimensionless circular frequency of TMF. We examine how variation of  $\gamma$  affects the TMF driving force, steady states, and the stability properties of the flow. The calculations are performed using the global Galerkin method described in Ref. [12].

It is known that with the increase of the TMF wavenumber, the time-averaged TMF driving force exhibits a significant skin-effect. We study how the flow varies with the TMF wavenumber and show that intensity of the TMF-induced vortex grows rapidly with the increase of the TMF wavenumber from a small value  $\alpha < 1$  to a moderate value  $1 < \alpha < 10$ , which depends on the aspect ratio and the TMF force amplitude. With further increase of  $\alpha$  the intensity slowly decreases. A similar change of the flow intensity is observed when the parameter  $\gamma$  is varied in the interval  $1 \leq \gamma \leq 20$ .

The present study shows that the dependence of the stability properties of the flow on the TMF wavenumber and the skin depth is rather complicated. The marginal stability curves contain non-monotonic parts with turning points and reinstatement of stability. Generally, the critical amplitude of the electromagnetic force steeply reduces with the increase of  $\alpha$  or  $\gamma$  from the value  $\alpha = 1$  ( $\gamma = 1$ ) and then slowly increases for  $\alpha > 10$  ( $\gamma > 10$ ), thus

behaves correspondingly to the increase or decrease of the intensity of the main TMF-induced vortex. The patterns of the most unstable perturbations show that the transition from an axisymmetric to the three-dimensional flow should be attributed to the instability of the main vortex and not to the thin skin-layer, even for large values of  $\alpha$  or  $\gamma$ .

## 2. Formulation of the problem

Consider flow of a Newtonian incompressible electrically conducting fluid in a cylindrical enclosure  $0 \leq r \leq R$ ,  $0 \leq z \leq H$  under action of a magnetic field traveling along the  $z$ -axis. It is assumed that at the cylindrical sidewall the vector potential of the magnetic field is given by

$$A_r = 0, \quad A_\theta = A_0 e^{i(\omega t - \tilde{\alpha} z)}, \quad A_z = 0, \quad (1)$$

where  $\tilde{\alpha}$  and  $\omega$  are the wavenumber and the circular frequency of the TMF.

Assuming that magnetic Reynolds number is small, the effect of the fluid flow on the magnetic field is neglected. Additionally, we assume that the flow is decomposed into time-averaged and oscillating parts and that the amplitude of the oscillating part is much smaller than that of the average part. This assumption is justified for large frequency of the magnetic field, which usually is about 50 Hz or even larger. Under the assumptions made, the time-averaged part of the flow is driven by a time-averaged electromagnetic force  $\mathbf{f}$  and is described by the dimensionless momentum and continuity equations:

$$\frac{\partial \mathbf{v}}{\partial t} + (\mathbf{v} \cdot \nabla) \mathbf{v} = -\nabla p + \Delta \mathbf{v} + \mathbf{f}, \quad (2)$$

$$\Delta \cdot \mathbf{v} = 0, \quad (3)$$

where  $\mathbf{v}$  is the fluid velocity and  $p$  is the pressure. The scales of length, time, velocity and pressure are  $R$ ,  $R^2/\nu$ ,  $\nu/R$  and  $\rho \nu^2/R^2$ , respectively, where  $\rho$  is the fluid density and  $\nu$  is the kinematic viscosity.

The expression for the electromagnetic force  $\mathbf{f}$  depends on a configuration of a magnetic field inductor. In the case of an infinite cylinder in an infinite inductor, the problem for the magnetic and

electric fields allows for an analytical solution, which yields the following expression for the time-averaged electromagnetic force [13]:

$$f_r = -Ft \frac{\text{Im}[I_1(\beta^*r)I_0(\beta r)]}{|I_0(\beta)|^2}, \quad f_\theta = 0, \\ f_z = Ft\alpha \frac{|I_1(\beta r)|^2}{|I_0(\beta)|^2}. \quad (4)$$

Here,  $Ft = A_0^2(\omega\sigma R^2/(2\rho v^2))$ ,  $\alpha = \tilde{\alpha}R$ ,  $\beta = \sqrt{\alpha^2 + i\gamma}$ ,  $\gamma = \sigma\omega\mu R^2$ , and  $\mu$  is magnetic permeability. An additional parameter defining the flow is the aspect ratio of the cylinder  $A = H/R$ . More complicated expressions, which take into account the finite extent of the inductor and the cylinder, as well as the distance between them, were obtained recently in Ref. [7]. It should be noticed that the radial component of the electromagnetic force (Eq. (4)) is potential and therefore does not affect the flow velocity. However, it is not small compared to the axial component and should be taken into account if correct pressure distribution is needed.

The electromagnetic force (Eq. (4)) is defined by three non-dimensional parameters: amplitude  $Ft$ , the parameter  $\gamma$  and the dimensionless axial wavenumber  $\alpha$ . For the following, we need to estimate the values of the dimensionless parameter  $\gamma$ , which can be interpreted as a dimensionless circular frequency of TMF. Note that in Ref. [4] and other papers  $K = \sqrt{\gamma}$  is called “skin depth” parameter. It follows from Eq. (4) that depth of the skin layer is defined by  $|\beta|$ , which is the function of both  $\alpha$  and  $\gamma$ , so that parameter  $\gamma$  alone is not enough to conclude about the skin layer depth (see also Fig. 1). Following the crystal growing experiments [10] and model RMF experiments [14], we estimate the characteristic length  $R$  to be 30 cm and the frequency of magnetic field to be 50 Hz. Then the parameter  $\gamma$  is approximately 0.426 for silicon melt ( $\sigma \approx 1.2 \times 10^6 \Omega^{-1} \text{m}^{-1}$ ) and 1.17 for InGaSn alloy ( $\sigma \approx 3.3 \times 10^6 \Omega^{-1} \text{m}^{-1}$ ). Thus, a characteristic value of the parameter  $\gamma$  can be taken as  $\gamma = 1$ . An increase of the parameter  $\gamma$  can be easily achieved by an increase of the TMF frequency. In the following, we also study the effect of variation of  $\gamma$  between the values 1 and 20 for the fixed value of  $\alpha = 1$ .

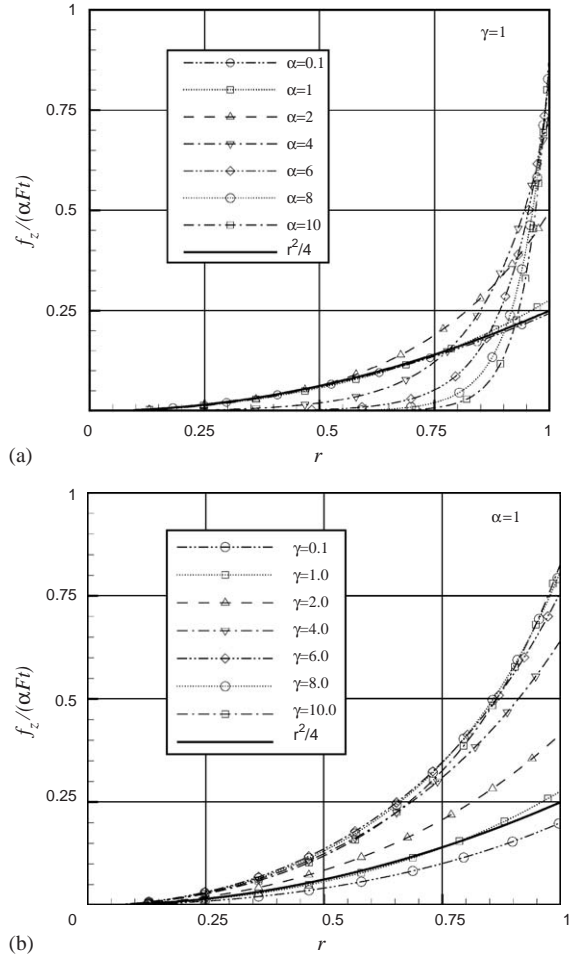


Fig. 1. Comparison of expressions (4) and (5) for the axial component of the time-averaged electromagnetic force.

The value of dimensionless wavenumber is equal to  $\alpha = 2\pi R/L$ , where  $L$  is the TMF wavelength. Obviously, at large  $L$  the wavenumber  $\alpha$  tends to zero. If the parameter  $\gamma$  is also small, so that  $|\beta| \ll 1$ , the expression for the  $z$ -component of the electromagnetic force (Eq. (4)) can be approximated asymptotically as

$$f_z = Ft\alpha|\beta|^2 \frac{r^2}{4} = Fb \frac{r^2}{4}, \quad Fb = B_0^2 \frac{\omega\sigma\tilde{\alpha}R^5}{2\rho v^2}, \quad (5)$$

where  $B_0 = A_0|\beta|/R$ . This expression was used for the stability analysis in Ref. [11] and parameter  $Fb$

Table 1

Critical parameter  $Fb_{cr}$  and critical circular frequency  $\omega_{cr}$  for the case of flow driven by the axial force (Eq. (5))

$N_r \times N_z$	$A = 1, k = 4$		$A = 2, k = 3$		$A = 4, k = 2$	
	$Fb_{cr} \times 10^{-6}$	$\omega_{cr}$	$Fb_{cr} \times 10^{-5}$	$\omega_{cr}$	$Fb_{cr} \times 10^{-5}$	$\omega_{cr}$
20 × 20	1.5673	634.20	4.8356	219.89	2.3167	105.15
30 × 30	1.5660	633.99	4.8184	219.06	2.3198	0
40 × 40	1.5660	633.98	4.8168	219.00	2.3200	0
50 × 50	1.5660	633.90	4.8168	218.97	2.3199	0
Result of Ref. [11]	1.5660	633.99	4.8176	219.03	2.3199	0

Table 2

Critical parameter  $Ft_{cr}$  and critical circular frequency  $\omega_{cr}$  for the case of flow driven by the axial force (Eq. (4))

$N_r \times N_z$	$\alpha = 1, k = 3$		$\alpha = 5, k = 2$		$\alpha = 10, k = 1$	
	$Ft_{cr} \times 10^{-5}$	$\omega_{cr}$	$Ft_{cr} \times 10^{-4}$	$\omega_{cr}$	$Ft_{cr} \times 10^{-4}$	$\omega_{cr}$
20 × 20	2.1799	217.45	1.1072	55.618	0.99309	86.225
30 × 30	2.1730	216.74	1.1072	55.618	0.99310	86.229
40 × 40	2.17245	216.71	1.1072	55.618	0.99310	86.229
50 × 50	2.17240	216.72	1.1072	55.618	0.99310	86.229

$A = 2.$

is equal to the doubled parameter  $F$  defined in Ref. [11]. In the following, we study the parametric dependence of the solution on the parameters  $\alpha$  and  $\gamma$ . Therefore, we prefer to use the governing parameter  $Ft$ , which is independent of  $\alpha$  and  $\gamma$ , instead of  $Fb$ .

In Fig. 1, we compare the force  $f_z$  for  $\gamma = 1$  and different  $\alpha$  (Fig. 1a), as well as for  $\alpha = 1$  and different  $\gamma$  (Fig. 1b), using expressions (4) and (5). For the exact comparison, the function  $r^2/4$  shown in Figs. 1a,b must be multiplied by  $|\beta|^2$ . It is clearly seen that with the increase of  $\alpha$  (Fig. 1a) the curves strongly differ by their shape. The difference in shapes is not so obvious in Fig. 1b; however, taking into account the factor  $|\beta|^2$  we can conclude that expression (5) yields overestimated values of the TMF force at large values of  $\gamma$  (e.g., at  $\gamma = 10$  the curve must be multiplied by  $\sqrt{101}$ ). At the same time, Eq. (5) still gives a good approximation when both  $\alpha$  and  $\gamma$  are close to unity. Eq. (4) must be accounted for already at  $\alpha = 2$  (Fig. 1a). For

$\alpha > 3$ , the force is characterized by a rapid growth near the cylinder wall ( $r = 1$ ), i.e. the well-known skin-effect is observed. Assuming that the TMF wavelength is of the order of the cylinder radius the value of  $\alpha$  can be estimated as  $2\pi$ , and exceeds 10 for  $L < R/2$ . The latter was the case of experiment [2].

For the present calculations, we consider  $1 \leq \alpha \leq 20$  for a fixed value  $\gamma = 1$ , which allows us to study the influence of the skin-effect on both flow patterns and their stability. Then we fix the wavenumber to be  $\alpha = 1$  and vary the parameter  $\gamma$  in the interval  $1 \leq \gamma \leq 20$ . For  $\alpha \leq 1$  and  $\gamma \leq 1$  the results of Ref. [11] apply. As in Ref. [11] we pose the no-slip boundary conditions on all the boundaries.

### 3. Numerical method

The problem is solved by the global Galerkin method. We applied the same numerical technique as was used in Refs. [15,16]. The flow is decomposed in the Fourier series

$$\langle \mathbf{v}, p \rangle = \sum_{k=-\infty}^{k=+\infty} \langle \mathbf{v}_k(r, z, t), p_k(r, z, t) \rangle \exp(ik\theta), \quad (6)$$

so that the term corresponding to  $k = 0$  describes both the axisymmetric base flow and the axisymmetric perturbation, and the terms with  $k \neq 0$  are used to describe all possible non-axisymmetric perturbations. Thus, the azimuthal wavenumber  $k$  plays a role of an additional integer parameter.

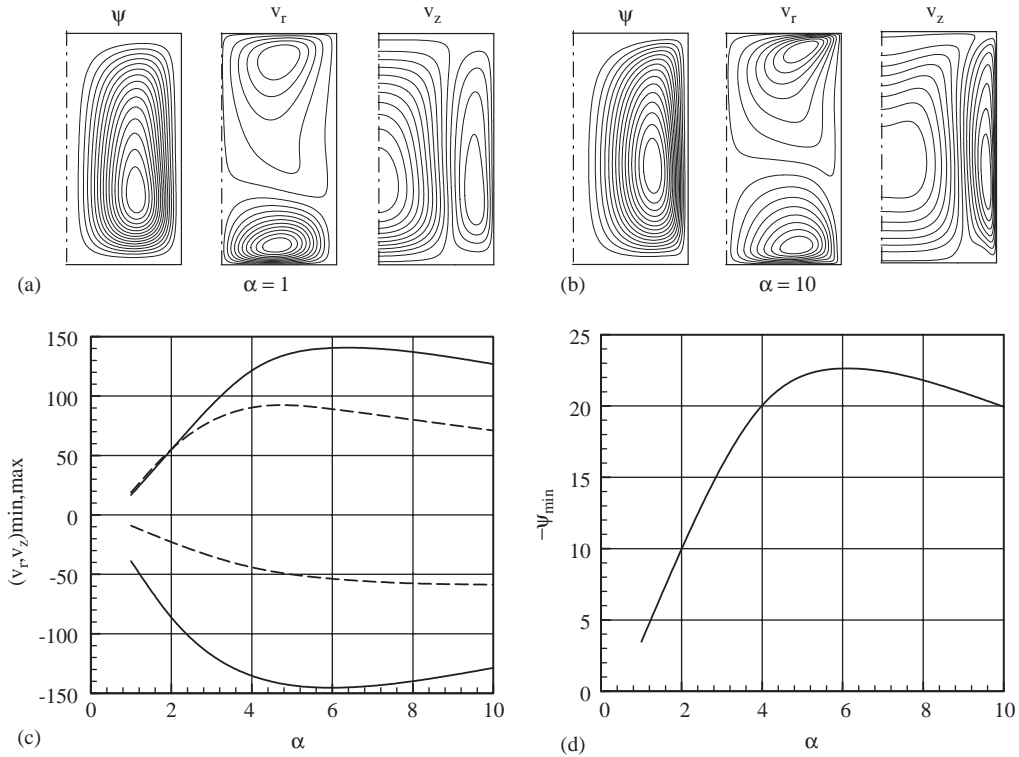


Fig. 2. Flow patterns for  $A = 2, \gamma = 1$ , and  $Ft = 10^4$ . (a, b) Patterns of the stream function, radial and axial velocities for  $\alpha = 1$  and 10, respectively; (c) dependence of the maximal and minimal values of the radial (dash lines) and axial (solid lines) velocities on the TMF wavelength  $\alpha$ ; (d) dependence of the minimal values of the stream function on the TMF wavelength  $\alpha$ .

The three-dimensional stability problem is considered for all non-negative values of  $k$ , and the critical forcing  $Ft_{cr}$  is defined as the minimum of all  $Ft_m(k)$  that correspond to a marginal stability limit for a given  $k$ . The functions  $\mathbf{v}_k(r, z, t)$ , defined in the meridional plane, are computed using the global Galerkin method. The pressure is excluded by the orthogonal Galerkin projections on the divergence-free velocity basis. The details on numerical method can be found in Ref. [12]. As in Refs. [15,16], the steady axisymmetric flow states were calculated by the Newton iteration. The eigenvalue problem related to the linear stability analysis of the calculated base states was solved using QR-decomposition algorithm. The critical parameters  $Ft_{cr}$  are followed by the values of critical circular frequency  $\omega_{cr}$ , which is the imaginary part of the leading eigenvalue of the

linear stability problem. The zero value of  $\omega_{cr}$  corresponds to a monotonically growing perturbation and indicates on a transition from one steady flow state to another. The non-zero value corresponds to a perturbation, whose amplitude growth is modulated by oscillations. In this case, one can expect a transition from steady to oscillatory flow state.

To ensure the correctness and the convergence, the present results were compared with those of Ref. [11] (Table 1), and then the convergence of the critical parameters for  $\alpha = 1, 5$  and 10 was examined for the force defined by Eq. (5) (Table 2). The tables show that the present results converge up to the third or fourth decimal digit already with the use of  $30 \times 30$  basis functions, and are in full agreement with the results of Ref. [11]. Therefore, the results reported below were

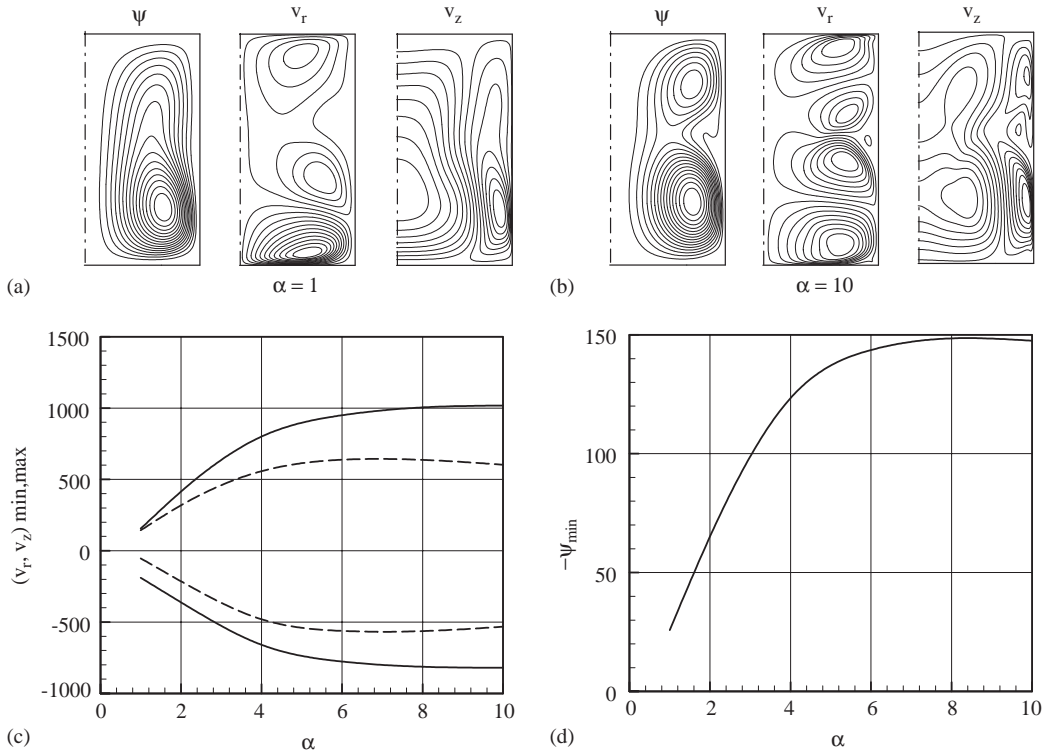


Fig. 3. Flow patterns for  $A = 2$ ,  $\gamma = 1$ , and  $Ft = 10^5$ . (a, b) Patterns of the stream function, radial and axial velocities for  $\alpha = 1$  and 10, respectively; (c) dependence of the maximal and minimal values of the radial (dash lines) and axial (solid lines) velocities on the TMF wavelength  $\alpha$ ; (d) dependence of the minimal values of the stream function on the TMF wavelength  $\alpha$ .

computed using  $30 \times 30$  basis functions in the  $r$ - and  $z$  directions.

#### 4. Results

Flow patterns at  $A = 2$ ,  $\gamma = 1$ ,  $\alpha = 1$  and 10 are shown in Figs. 2 and 3 for  $Ft = 10^4$  and  $10^5$ , respectively. In all cases, the flow rises along the cylindrical sidewall and descends along its axis. All the isolines are equally spaced between the minimal and maximal values of the stream function  $\psi$ , radial velocity  $v_r$  and axial velocity  $v_z$ . The maximal and minimal values of the velocities and the stream function are shown in the frames (c) and (d) as functions of the TMF wavenumber  $\alpha$ . Obviously, for negative values of  $\alpha$ ,

the flows can be obtained by turning over the frames.

At a moderate amplitude of the electromagnetic force  $Ft = 10^4$  (Fig. 2), the shape of flow pattern remains almost unchanged with the growth of the wavenumber  $\alpha$ , except a growing concentration of isolines of  $\psi$  and  $v_z$  near the cylindrical sidewall due to the skin-effect. The examination of the minimal and maximal values (Fig. 2c,d) shows that the flow intensity grows with the increase of the wavenumber up to  $\alpha \approx 6$  and then starts to decrease. The decrease can be explained by the decrease of the average force, which can be defined as  $\int_0^1 f_z(r) dr$  (see Fig. 1).

At larger electromagnetic force amplitude  $Ft = 10^5$  (Fig. 3), the shape of flow patterns start to change with the wavenumber. For  $\alpha \geq 6$ , the

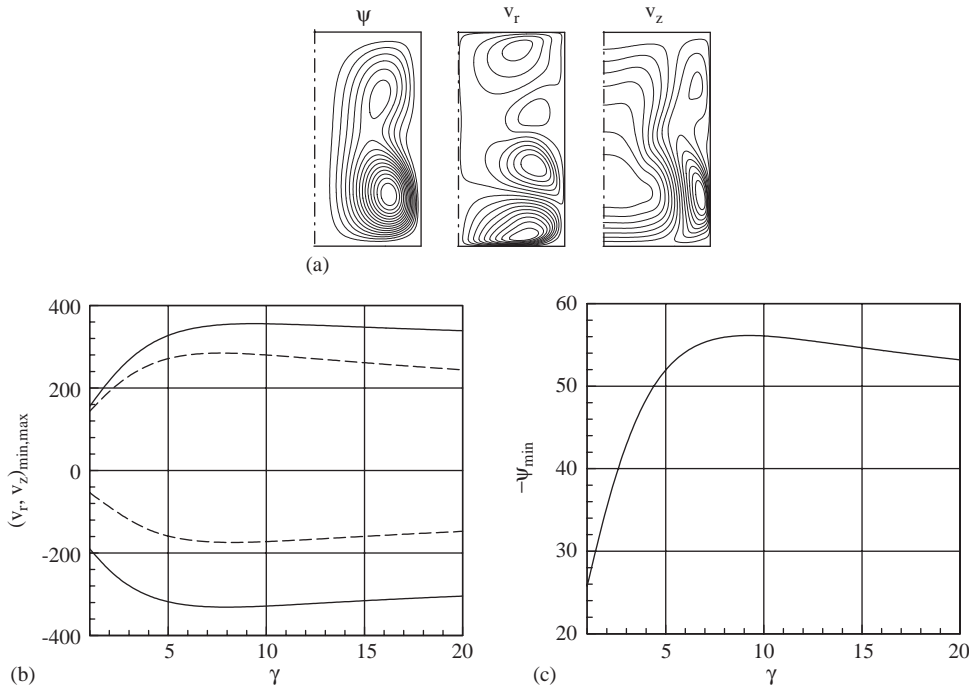


Fig. 4. (a) flow pattern for  $A = 2$ ,  $\alpha = 1$ ,  $\gamma = 10$  and  $Ft = 10^5$ ; (b) dependence of the maximal and minimal values of the radial (dash lines) and axial (solid lines) velocities on the TMF wavelength  $\gamma$ ; (c) dependence of the minimal values of the stream function on the TMF wavelength  $\gamma$ .

axial velocity attains a rather sharp minimal value near the sidewall midpoint (Fig. 3b), however does not change its positive sign, so that the flow retains its upward direction along the sidewall. As in the previous case, the intensity of the flow grows with the increase of the wavenumber (Fig. 3c,d), and then, starting from the value  $\alpha = 10$ , decreases. Note that according to the stability results described below steady flows at  $Ft = 10^5$  and  $\alpha > 1.2$  are unstable with respect to steady or oscillatory three-dimensional perturbations.

Fig. 4a depicts the flow pattern for  $\alpha = 1$  and  $\gamma = 10$ . The flow pattern does not change significantly compared to the patterns at  $\gamma = 1$  and larger  $\alpha$ . Figs. 4b and c show how the maximal values of the velocity components and the stream function change with the increase of the parameter  $\gamma$ . Similar to the increase of  $\alpha$  the flow intensity increases when  $\gamma$  grows starting from the value

$\gamma = 1$  and then slowly decreases beyond the value  $\gamma = 10$ .

The three-dimensional instability of the base axisymmetric flows was studied for the aspect ratios  $A = 1, 2, 3$  and 4. In the first series of calculations, the value of parameter  $\gamma$  was fixed at  $\gamma = 1$  and the TMF wavenumber  $\alpha$  was varied from 1 to 20. Then the wavenumber was fixed at  $\alpha = 1$  and the parameter  $\gamma$  was varied between 1 and 20. As mentioned above, the stability analysis is carried out separately for different values of the azimuthal wavenumber  $k$ .

The marginal stability curves for the considered values of the aspect ratio,  $\gamma = 1$  and the wavenumber  $k$  varying from 0 to 6 are shown in Fig. 5. For all considered values of  $A$  and  $k$ , the dependencies  $Ft_m(\alpha)$  are characterized by a rapid decrease of  $Ft_m$  when the wavenumber  $\alpha$  is varied from 1 to approximately 6 and a slow increase after reaching the minimal value.

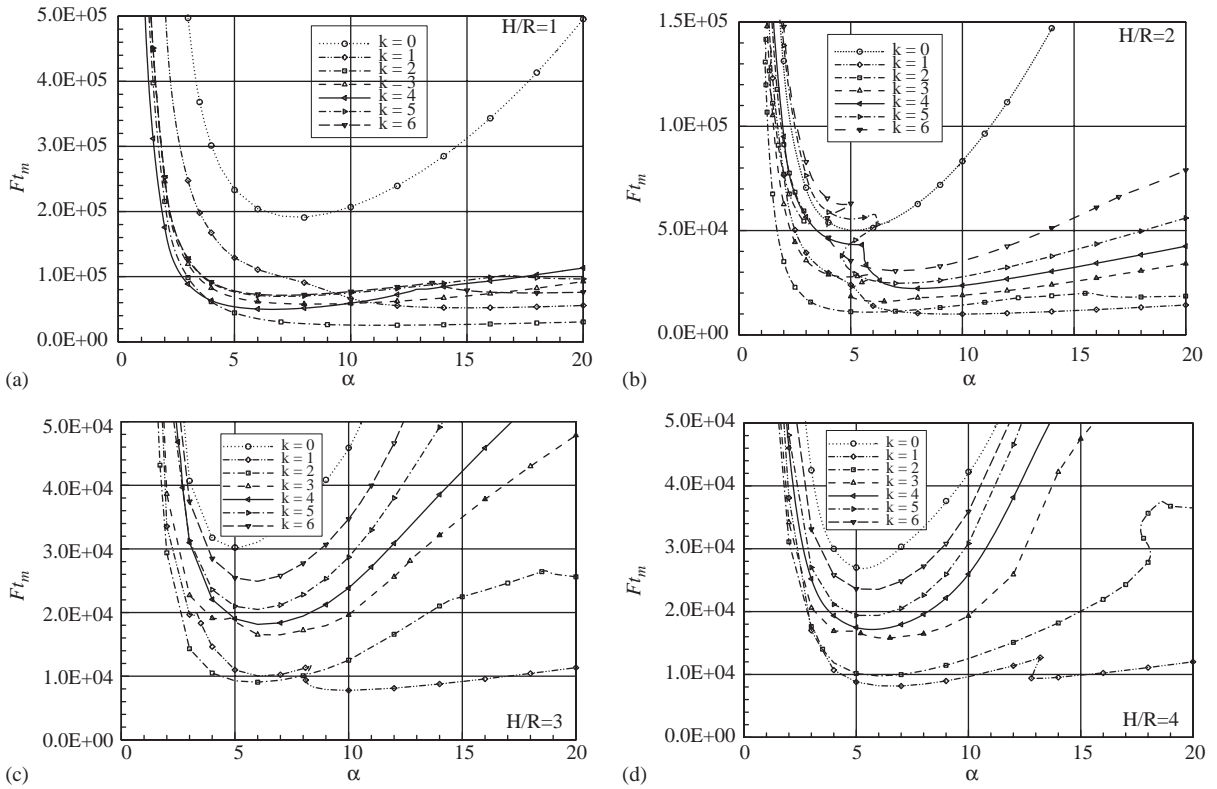


Fig. 5. Marginal stability curves for three-dimensional instability of flows at aspect ratios  $A = H/R = 1-4$ ,  $\gamma = 1$ .

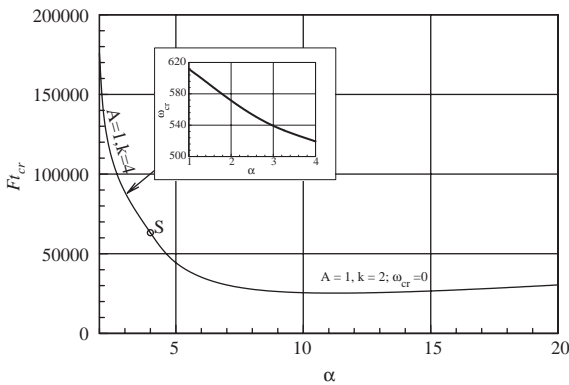


Fig. 6. Critical curve for  $A = 1$ ,  $\gamma = 1$ .

Most marginal curves are smooth. At the same time there are several marginal curves containing turning points, e.g. curves correspond-

ing to  $k = 3$  and  $6$  in Fig. 5b. This non-monotonic behavior does not necessarily affect the stability limits, but can lead to a complicated non-linear dynamics in the unstable three-dimensional regimes.

The critical values of  $Ft$  correspond to the lower envelope of the marginal curves corresponding to different  $k$ . It is seen (Fig. 5) that the most critical perturbation is never axisymmetric, so that the onset of instability always leads to a transition from an axisymmetric to a three-dimensional flow. The lower envelopes are shown in Figs. 6–8. For the cases of oscillatory instability, the critical circular frequencies  $\omega_{cr}$  are shown in Figs. 6–8 as insets.

At  $A = 1$  (Fig. 6) and small values of the TMF wavenumber,  $\alpha < 4$ , the critical mode is oscillatory and corresponds to the azimuthal wavenumber  $k = 4$ . With the increase of  $\alpha$ , at the point S in

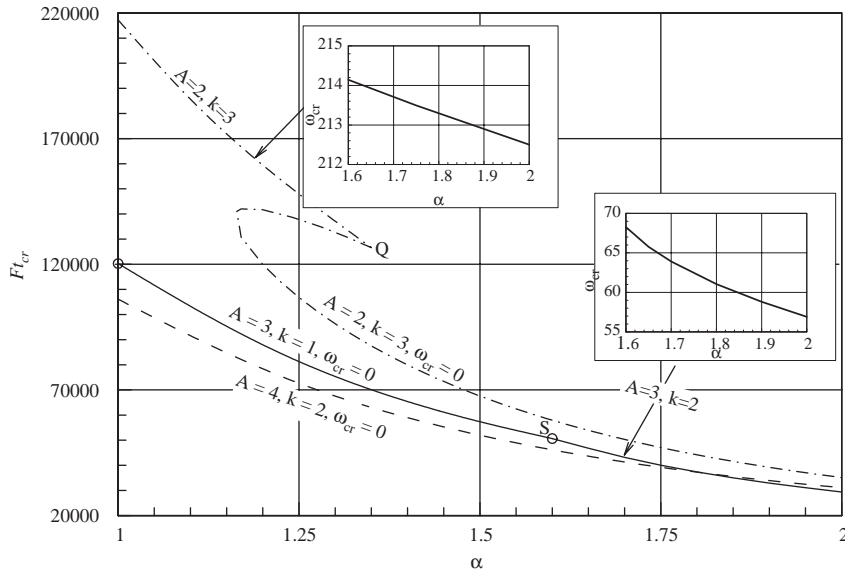


Fig. 7. Critical curves for  $A = 2, 3$  and  $4; \gamma = 1, 1 \leq \alpha \leq 2$ .

Fig. 6, the critical mode switches to a stationary one with  $k = 2$ .

The non-monotonic behavior of the critical curve is observed for  $A = 2$  and  $1 \leq \alpha \leq 2$  (Fig. 7). Here, close to the value of TMF wavenumber  $\alpha = 1.25$  we observe the reinstatement of stability. The flow becomes unstable due to the stationary mode  $k = 3$ , then stability reestablishes at larger value of  $Ft$ , and with the further increase of  $Ft$  the instability sets in due to the oscillatory mode with  $k = 3$ . The switch between the two modes takes place at the point Q (Fig. 7). Note that these two modes have the same azimuthal periodicity, but different spatial patterns and temporal behavior. The critical curves in the cases  $A = 3$  and  $4$  are smooth in the interval  $1 \leq \alpha \leq 2$  (Fig. 7). A switch between the steady mode with  $k = 1$  and the oscillatory mode with  $k = 2$  is observed at the point S in the case  $A = 3$ . At larger values of  $\alpha$  we observe several replacements of the most critical modes, which are indicated by the letters Q, R and S in Fig. 8. At  $A = 3$  and  $4$ , we observe also narrow intervals containing turning points and reinstatement of stability, which are similar to one discussed above for the case  $A = 2$ . With the

increase of the aspect ratio these intervals shift in the area of larger  $\alpha$ .

The isolines of the amplitudes of the three-dimensional perturbations, which are functions of  $r$  and  $z$  only, are shown in Fig. 9. It should be noted that in spite of the strong concentration of the driving force near the cylindrical wall (Fig. 1) the perturbations are distributed over whole flow region. Only at  $\alpha = 1$  the patterns are shifted toward the wall. At large  $\alpha$ , i.e.  $\alpha = 10$  and  $20$ , the perturbation patterns cover the whole flow region, indicating the instability of the whole vortex rather than an instability of the boundary layer. At  $\alpha = 10$ , one can observe weak maxima of the perturbation amplitude adjacent to the cylindrical wall. This can be a sequence of the skin-effect, however these local maxima are much weaker than the global ones.

Figs. 10–12 show the lower envelopes of the marginal stability curves for the fixed value  $\alpha = 1$  and varying parameter  $\gamma$ . As above, the non-zero critical frequency is shown in the insets. It is seen that the dependencies  $Ft_{cr}(\gamma)$  are similar to the dependencies  $Ft_{cr}(\alpha)$ . Starting from small values of  $\gamma$ , the critical values of the parameter  $Ft$

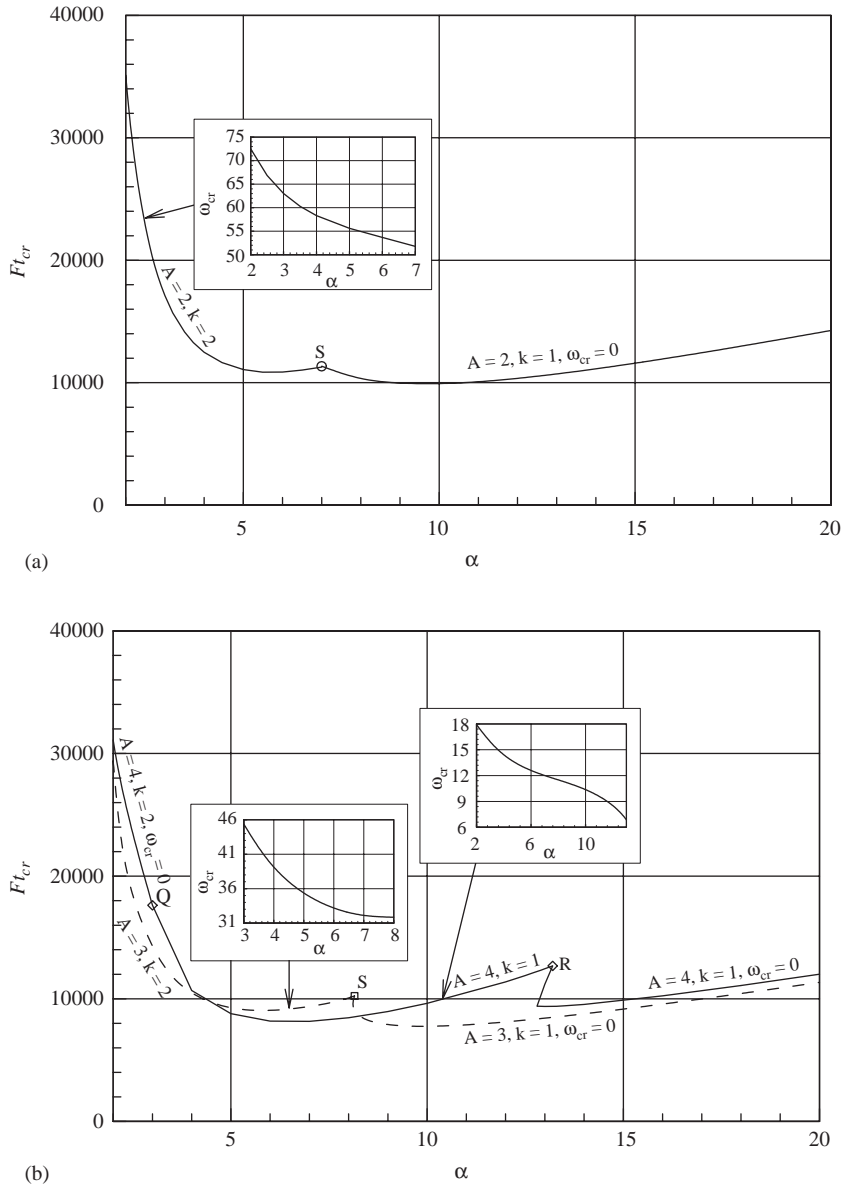


Fig. 8. Critical curves for  $A = 2, 3$  and  $4; \gamma = 1, 2 \leq \alpha \leq 20$ .

sharply decrease and change slowly for  $\gamma > 10$ . At  $A = 2$ , we again observe a non-monotonic behavior of the neutral curve with two turning points and the reinstatement of stability (cf. Figs. 7 and 11).

### 5. Conclusions

The patterns and three-dimensional stability of axisymmetric time-averaged flows driven by the TMF were studied numerically. The dependence of

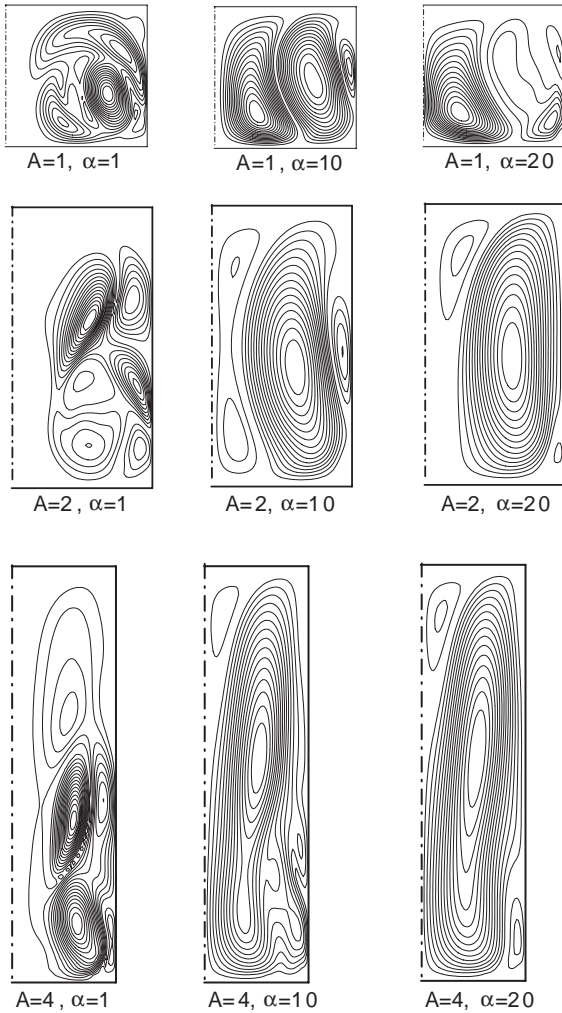


Fig. 9. Amplitudes of the 3D perturbation of axial velocity.

the flows and their stability properties on the TMF wavenumber  $\alpha$  and the dimensionless TMF frequency  $\gamma$  was examined. It was shown that an increase of  $\alpha$  (or  $\gamma$ ) from  $\alpha = 1$  (or  $\gamma = 1$ ) to a moderate values of  $\alpha = 5-10$  (or  $\gamma = 10$ ), depending on the aspect ratio of the flow region, leads to an intensification of the flow and reduces the critical value of the TMF force amplitude  $Ft_{cr}$ . Further increase of the TMF wavenumber leads to the flow slowdown and then to a slow increase of  $Ft_{cr}$ , which is observed for  $\alpha > 10$  (or  $\gamma > 15$ ).

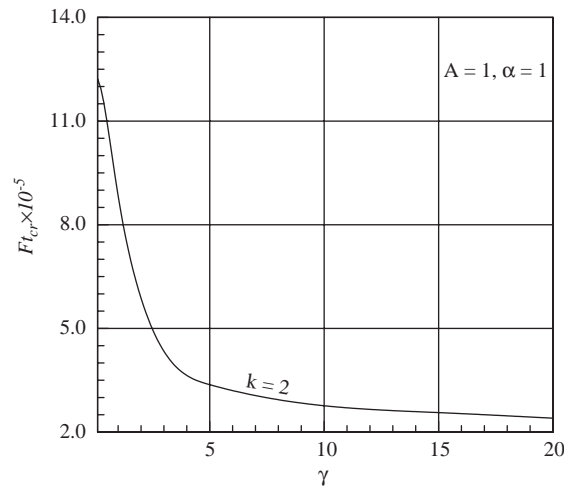


Fig. 10. Critical curve for  $A = 1, \alpha = 1$ .

It was found that the dependencies  $Ft_{cr}(\alpha)$  and  $Ft_{cr}(\gamma)$  are not always smooth and sometimes can contain turning points and reinstatement of stability, so that the axisymmetric base flow can become unstable at  $Ft_{cr}^{(1)}$ , then stable at  $Ft_{cr}^{(2)} > Ft_{cr}^{(1)}$ , and finally unstable at  $Ft_{cr}^{(3)} > Ft_{cr}^{(2)}$ . This can lead to a complicated dynamics in the supercritical regimes and should be taken into account if time-dependent calculations are performed.

On the basis of the patterns of the most unstable three-dimensional perturbations, it was concluded that the transition from an axisymmetric to a three-dimensional flow state takes place due to instability of the whole TMF-induced vortex, and not due to disturbances developing in the skin-layer.

Obviously, when the TMF is used for the control of melt flow in a crystal growth process, the TMF-induced force should be considered together with other forces, which drive the melt flow, e.g. buoyancy, thermocapillary or centrifugal forces. The interaction of several driving forces can lead to drastic changes in the flow patterns and especially in the stability properties of the flow. The present analysis would be applicable in cases when the TMF driving force is significantly larger than all other forces.

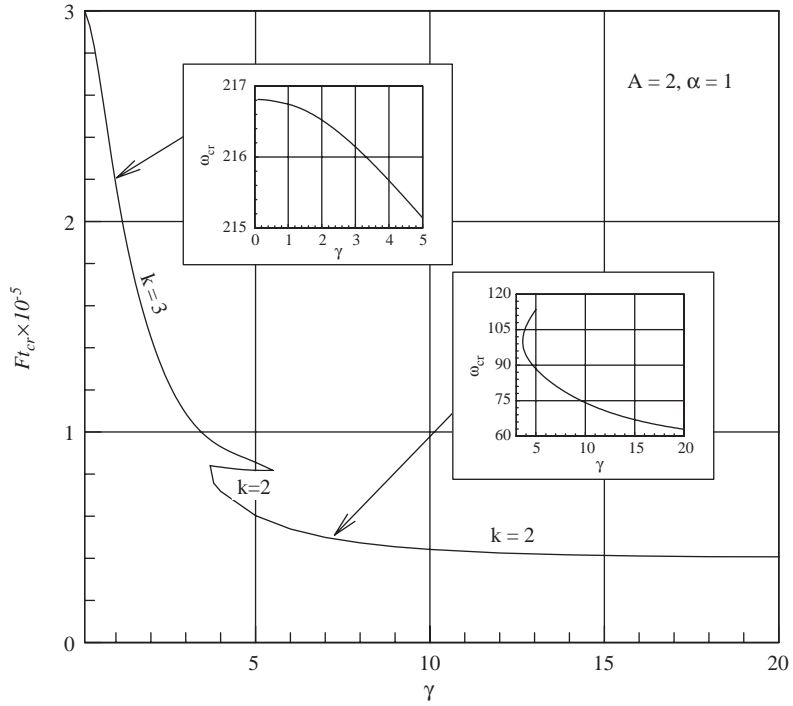


Fig. 11. Critical curve for  $A = 2, \alpha = 1$ .

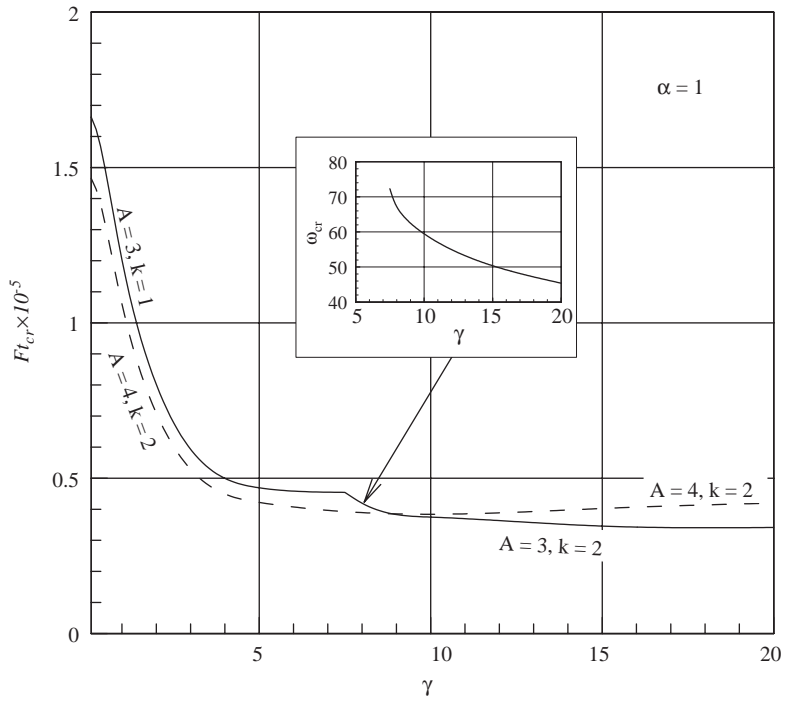


Fig. 12. Critical curve for  $A = 3$  and  $4, \alpha = 1$ .

## Acknowledgments

This study was supported by the German-Israeli Foundation, Grant no. 1-794-145.10/2004. The author thanks Dr. I. Grants for providing his numerical data for comparison.

## References

- [1] Yu. Gelfgat, J. Krūminš, M. Abricka, *Magnetohydrodynamics* 36 (1999) 3.
- [2] N. Ramachandran, K. Mazuruk, M.P. Volz, *SPIE* 3792 (1999) 39.
- [3] M. Abricka, Yu. Gelfgat, J. Krūminš, *Energy Convers. Manage.* 43 (2002) 327.
- [4] K. Mazuruk, *Adv. Space Res.* 29 (2002) 541.
- [5] Yu. Gelfgat, J. Krūminš, M. Abricka, *Magnetohydrodynamics* 39 (2003) 201.
- [6] V. Socoliuc, D. Vizman, B. Fischer, J. Friedrich, G. Müller, *Magnetohydrodynamics* 39 (2003) 187.
- [7] M.P. Volz, K. Mazuruk, *Magnetohydrodynamics* 40 (2004) 117.
- [8] T.P. Lyubimova, A. Croell, P. Dold, O.A. Khlybov, I.S. Fayzrakhmanova, *J. Crystal Growth* 266 (2004) 404.
- [9] P. Schwesig, M. Hainke, J. Friedrich, G. Mueller, *J. Crystal Growth* 266 (2004) 224.
- [10] E. Tomzig, J. Virbulis, W. von Ammon, Yu. Gelfgat, L. Gorbunov, *Mater. Sci. Semicond. Process.* 5 (2003) 347.
- [11] I. Grants, G. Gerbeth, *J. Crystal Growth* 269 (2004) 630.
- [12] A.Yu. Gelfgat, *CFD J.* 9 (2001) 437.
- [13] J. Krūminš, *Fundamentals of Theory and Calculation for Devices with a Traveling Magnetic Field*, Zinātne Publishing House, Riga, 1983 (in Russian).
- [14] Yu.M. Gelfgat, A.Yu. Gelfgat, *Magnetohydrodynamics* 40 (2004) 147.
- [15] A.Yu. Gelfgat, P.Z. Bar-Yoseph, A. Solan, *J. Crystal Growth* 220 (2000) 316.
- [16] A.Yu. Gelfgat, P.Z. Bar-Yoseph, A. Solan, *J. Crystal Growth* 230 (2001) 63.